JOURNAL OF GEOPHYSICAL RESEARCH, VOL. 113, E12011, doi:10.1029/2008JE003076, 2008

Origin of the Medusae Fossae Formation, Mars: Insights from a synoptic approach

Kathleen E. Mandt,[1,2] Shanaka L. de Silva,[3] James R. Zimbelman,[4] and David A. Crown[5]

Received 29 January 2008; revised 17 June 2008; accepted 19 August 2008; published 20 December 2008.

[1] The geologic origin of the Medusae Fossae Formation (MFF) has remained a mystery despite three decades of research. To better constrain its formation, an in-depth analysis of observations made in the literature was combined with a new survey of over 700 Mars Orbiter Camera narrow-angle images of the MFF to identify morphologic characteristics and material properties that define this formation as a whole. While previous work has identified clear agreement on some characteristics, our analysis identifies yardangs, collapse features, and layering as pervasive features of the MFF. Whereas collapse features and layering may implicate several different physical and chemical processes, yardangs provide vital information on material properties that inform about mechanical properties of the MFF lithology. Aspect ratios of megayardangs range from 3:1 to 50:1, and slope analyses reveal heights of up to 200 m with cliffs that are almost vertical. Other yardangs show lower aspect ratios and topographic profiles. These characteristics coupled to the presence of serrated margins, suggest that MFF lithology must be of weakly to heavily indurated material that lends itself to jointing. The characteristics and properties of the MFF are inconsistent with those of terrestrial pyroclastic fall deposits or loess, but are in common with large terrestrial ignimbrites, a hypothesis that explains all key observations with a single mechanism. Yardang fields developed in regionally extensive ignimbrite sheets in the central Andes display morphologic characteristics that correlate with degree of induration of the host lithology and suggest an origin by pyroclastic flow for the MFF.

Citation: Mandt, K. E., S. L. de Silva, J. R. Zimbelman, and D. A. Crown (2008), Origin of the Medusae Fossae Formation, Mars: Insights from a synoptic approach, *J. Geophys. Res.*, *113*, E12011, doi:10.1029/2008JE003076.

1. Introduction

[2] The Medusae Fossae Formation (MFF) is an enigmatic deposit located along the equator of Mars that stretches between 170 and 240°E (120–190°W) in the Amazonis Planitia region and lies between the Tharsis and Elysium volcanic centers (Figure 1). The MFF has been a focus of nearly three decades of research because its age, distribution, and material properties have important implications for Martian history. It is considered to be one of the youngest deposits on Mars, largely Amazonian in age, but deposition may have begun as early as the Hesperian Period [*Scott and Tanaka*, 1986; *Greeley and Guest*, 1987; *Tanaka*, 2000; *Head and Kreslavsky*, 2001, 2004]. However, despite general agreement about the relatively young age and fine-grained nature of the MFF materials, its origin is still debated and a variety of disparate hypotheses have been proposed, including deposition by pyroclastic flows [*Scott and Tanaka*, 1982, 1986; *Tanaka*, 2000] or falls [*Tanaka*, 2000; *Bradley et al.*, 2002; *Hynek et al.*, 2003], aeolian deposits [*Greeley and Guest*, 1987; *Scott and Tanaka*, 1986; *Head and Kreslavsky*, 2004], polar deposits [*Schultz and Lutz*, 1988], exhumed faulted rocks [*Forsythe and Zimbelman*, 1988], carbonate platform [*Parker*, 1991], rafted pumice [*Mouginis-Mark*, 1993], lacustrine deposits [*Malin and Edgett*, 2000], and as deposits from meteorite impact into a subsurface aquifer [*Nussbaumer*, 2005].

2. Evaluation

[3] To bring some clarity to this issue, we have compiled and analyzed all the published information on the MFF in search of an approach that may help advance the debate. We note that some hypotheses have not been published in the peer reviewed literature. Several hypotheses have been eliminated on the basis of subsequent work (Table 1). For instance, the demonstrably Amazonian age, if correct, of the MFF [*Scott and Tanaka*, 1986; *Greeley and Guest*, 1987; *Tanaka*, 2000; *Head and Kreslavsky*, 2001, 2004] is inconsistent with the paleopolar deposit, exhumed faulted rocks, and lacustrine deposit hypotheses because each of these

[1]Department of Space Studies, University of North Dakota, Grand Forks, North Dakota, USA.
[2]Now at Space Science and Engineering Division, Southwest Research Institute, San Antonio, Texas, USA.
[3]Department of Geosciences, Oregon State University, Corvallis, Oregon, USA.
[4]Center for Earth and Planetary Sciences, National Air and Space Museum, Smithsonian Institution, Washington, District of Columbia, USA.
[5]Planetary Science Institute, Tucson, Arizona, USA.

0148-0227/08/2008JE003076$09.00

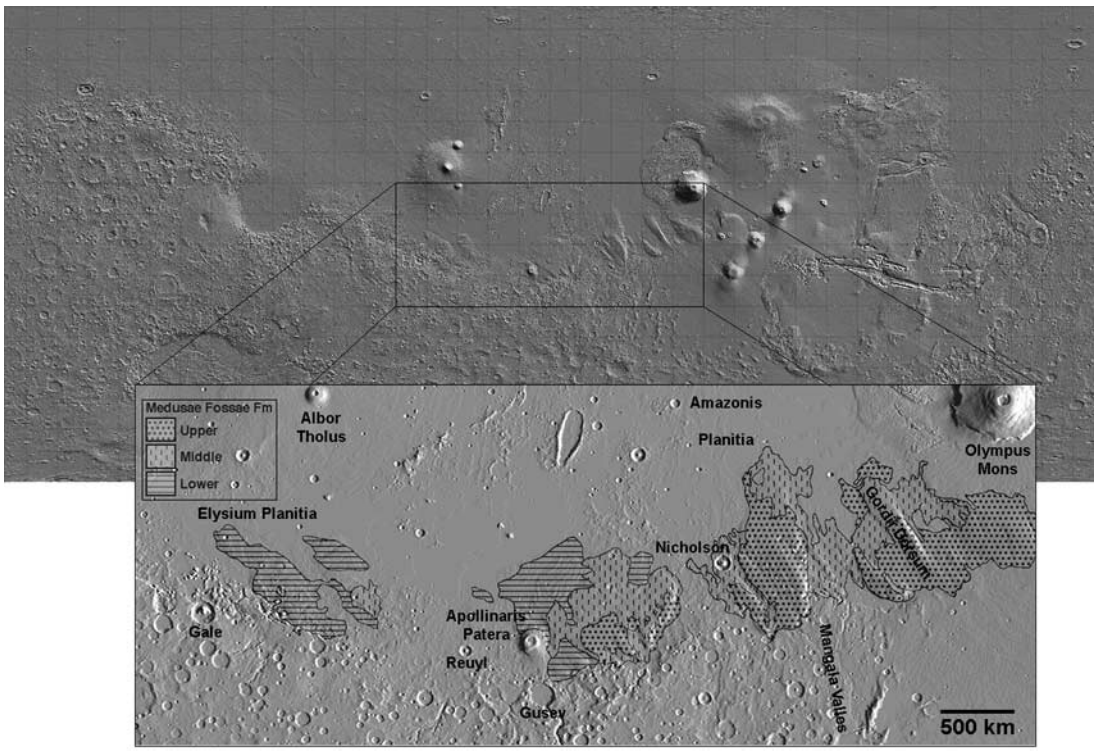

Figure 1. Map of the Medusae Fossae Formation overlain on MOLA shaded relief 128 pixel/° digital elevation model (DEM) (shown in context with MOLA shaded relief centered around 180°E and 0°N). MFF subdivisions of upper, middle, and lower are based on mapping by *Scott and Tanaka* [1986] and *Greeley and Guest* [1987].

requires the MFF to have a Noachian or Early Hesperian formation age. Improved resolution provided by Mars Global Surveyor (MGS) and topographic data from the Mars Orbiter Laser Altimeter (MOLA) have ruled out the carbonate platform hypothesis. The type of layering expected in a carbonate platform is not seen in the MFF [*Bradley et al.*, 2002]. The rafted pumice deposit hypothesis was contradicted by the same data because no wave-cut cliffs were seen on Olympus Mons [*Malin*, 1999]. We find that, of the original nine hypotheses, only three are still

Table 1. Hypotheses for the MFF

Hypothesis	Basis	Source	Ruled Out By
Ignimbrite/ash flow tuff	Similarities to ignimbrites in the Pancake Range of Nevada	*Scott and Tanaka* [1982]	
Aeolian deposit	location along dichotomy boundary	*Greeley and Guest* [1987]	
Paleopolar deposits	similarities to current polar deposits	*Schultz and Lutz* [1988]	MFF is same age as current polar deposits, and polar wander is limited on the basis of fault patterns [*Tanaka and Leonard*, 1998] Morphological differences in slopes and valleys of MFF compared to current polar deposits [*Bradley et al.*, 2002]
Exhumed fault rocks	as support for proof of dynamic tectonic activity	*Forsythe and Zimbelman* [1988]	MFF must be Noachian for this hypothesis [*Scott and Tanaka*, 1986; *Greeley and Guest*, 1987]
Carbonate platform	similar morphology to terrestrial carbonate platforms	*Parker* [1991]	topography too complex and layering not appropriate [*Sakimoto et al.*, 1999; *Bradley et al.*, 2002] and Thermal Emission Spectrometer (TES) data [*Chapman*, 2002]
Rafted pumice deposits	signs on Olympus Mons of suboceanic volcanism	*Mouginis-Mark* [1993]	layering not like a shoreline deposit and no wave-cut cliffs in Olympus Mons [*Malin*, 1999; *Bradley et al.*, 2002]
Lacustrine deposits	outcrops resembling sedimentary rock	*Malin and Edgett* [2000]	age must be Noachian for this hypothesis [*Scott and Tanaka*, 1986; *Greeley and Guest*, 1987]
Ashfall tuff	draped over underlying terrain	*Tanaka* [2000] *Bradley et al.* [2002] *Hynek et al.* [2003]	
Subsurface aquifer	evidence of glacial activity, ground moraines, and sublimation	*Nussbaumer et al.* [2005]	supporting evidence cited is contradictory

Table 2. Analysis of Literature[a]

		Extrinsic							Intrinsic Properties			
		Processes		Transportation Mechanisms								
Category	Feature	Erosional	Depositional	Aeolian	Subteranian	Sublimation	Fluvial	Glacial	Fine Grained	Jointed	Indurated	Friable
Large Scale												
	Volume (large volume of material)		3, 12, 25									
	Thick (up to 3 km in some places)		8, 9, 10, 25, 28									
	Increased relief toward Tharsis		11									
	Thickness trends increase toward Tharsis		12									
	Young based on stratigraphic relations		2, 8, 9, 10, 28									
	Outlying yardang fields, pedestal craters and mounds within craters		3, 9, 10, 12, 17	9, 12, 17		10			16			3
	Complex stratigraphy indicating multiple episodes of deposition		9	9								
	Underlying terrain not modified		12, 16, 23, 29	12					16			16
	Interweaving of lava and MFF deposition		16									
	Mesas	3, 30		30								
	Steep cliffs	18, 25									18, 25	
	Serrated scarps	8, 26		8, 26								
	Teardrop-shaped hills separated by large valleys	9, 10										
	Fish-scale-like knobs and curvilinear troughs	19			19							
	Rough, hackly surface	25									25	
	Lack of boulders along erosional contacts	12, 18		12, 18					12, 18			
	Wide range of roughness characteristics	7		7							7	
	Irregular topography	27		27								
	Smooth surfaces with broadly curved margins		25									25
	Unconformably overlies dichotomy boundary and aureole deposits		9, 10									
	Boundary terraces flat, not conforming to topography		25									
Linear												
	Yardangs	2, 3, 4, 8, 12, 18, 23, 25, 26, 27, 28, 30		2, 3, 4, 8, 12, 18, 23, 25, 26, 27, 28, 30				20	18, 27		18, 24, 25	3, 4, 23, 26, 27, 30
	Bidirectional yardangs	4, 25		4, 25						4, 25	25	4
	Troughs	9, 10		9, 10		10						
	Ridges and grooves	8, 17, 26		8, 17, 26								
	Chutes or dark scree slopes	12		12			12		12			12
	Flutes	12, 30		12, 30								
	Corrugated texture	19		19							24	19
	Intersecting blocky layers	4								3, 4	4	
	Hummocky terrain		20					20				
	Surface cuestas and undulations	6			6							
	Wind streaks	30		30								
	Viscous flow features	19, 21				21	19					
	Raised curvilinear features	5, 9, 10	5, 20, 21	5			5, 9, 10, 20, 21	5, 20, 21				

Table 2. (continued)

		Extrinsic							Intinsic Properties			
		Processes		Transportation Mechanisms								
Category	Feature	Erosional	Depositional	Aeolian	Subteranian	Sublimation	Fluvial	Glacial	Fine Grained	Jointed	Indurated	Friable
Circular												
	Impact crater depth-diameter ratios								1			1
	Large secondary craters								24			
	Extensive secondary fields around primary craters								24			
	Double-ringed exhumed craters	9, 10		9		10			27			
	Craters between layers		11, 12, 27						27			
	Impact craters on remnant mesas		17								17	
	Pedestal craters	9, 10, 14, 24, 25, 30		24, 25, 30		10, 14			14			
	Low rims of superposed craters		25									25
	Knobs	3, 24, 25	20, 21	24, 25			20, 21	20, 21			24, 25	
Semicircular												
	Crescent-shaped dunes	24		24								24
	Horseshoe wind streaks	34		34					34			
Depressions												
	V-shaped depressions	3		3								3
	Irregular flat-floored depressions	24		24							24	
	Fluvial channels visible through deposit		3, 4, 33									
	Erosional pitting	22					22					
	Collapse features	19	25		19, 25							
Layering												
	Topographic slope breaks coincident with albedo shifts	3, 4, 23									3, 4	3, 4
	Changing yardang orientation	30, 31, 32	3, 12, 25	3, 30, 32						31	3, 25	
	Patterns visible beneath partly eroded cover	25										
	Stair steps	18										
	Cliff benches	18										
	Banded terrain	18										
	Mesa-to-mesa common elevation range		23									
	Lower albedo where linear ridges are visible	25, 26										
	Horizontal layer in cliff with lower temperature		32									
	Albedo shifts	6			6							
	Uniform, gradual slopes (no layering)		2									
Remote sensing												
	Gamma Ray Spectrometer measurements		13, 15									
	Viking infrared thermal mapper and TES (low thermal interia)		12, 28						12, 28			
	Little to no radar signature		16, 22						16, 22			

[a]Numbers in the body of the table refer to the following references: 1, *Barlow* [1993]; 2, *Bradley et al.* [2000]; 3, *Bradley and Sakimoto* [2001]; 4, *Bradley et al.* [2002]; 5, *Burr et al.* [2006]; 6, *Forsythe and Zimbelman* [1988]; 7, *Frey et al.* [1998]; 8, *Greeley and Guest* [1987]; 9, *Head and Kreslavsky* [2001]; 10, *Head and Kreslavsky* [2004]; 11, *Hynek et al.* [2002]; 12, *Hynek et al.* [2003]; 13, *Ivanov et al.* [2005]; 14, *Kadish and Barlow* [2006]; 15, *Keller et al.* [2006]; 16, *Lanagan and McEwan* [2003]; 17, *Malin et al.* [1998]; 18, *Malin and Edgett* [2000]; 19, *McColley et al.* [2005]; 20, *Nussbaumer et al.* [2003]; 21, *Nussbaumer* [2005]; 22, *Parker* [1991]; 23, *Sakimoto et al.* [1999]; 24, *Schultz and Lutz* [1988]; 25, *Scott and Tanaka* [1982]; 26, *Scott and Tanaka* [1986]; 27, *Takagi and Zimbelman* [2001]; 28, *Tanaka* [2000]; 29, *Zimbelman et al.* [1997b]; 30, *Zimbelman and Patel* [1998]; 31, *Zimbelman et al.* [2000]; 32, *Zimbelman* [2003]; 33, *Zimbelman et al.* [2003]; and 34, J. R. Zimbelman (personal communication, 2007).

Table 3. Characteristics of Yardangs on Earth and the MFF

Location	Lithology	Yardang Characteristics	Aspect Ratio (length:width)
Iran, Lut Desert[a]	silty clays, gypsiferous sands moderately indurated	10s of km long, 60–80 m tall	
Peru, Pisco Formation[b]	marine sediments		
China, Lop Nor[a,c]	lake beds	100s of meters long, 20 m high	up to 10:1
Rogers Lake, CA, USA[d]	gravel, sand, silt, and clay moderately consolidated		5:1
Egypt, Western Desert[c,e]	silicified limestone, lake beds, chalk	10–100 m long, 2–5 m tall	
Chad[e]	indurated sandstone	20–30 km long, 1 km wide; spacing 500 m to 2 km	20:1–30:1
Argentina, Payun Matru[f]	ignimbrites and lavas	2–10 km long; lavas result in broad troughs; Ignimbrites yardangs	
N. Saudi Arabia[c]	Cambrian sandstone	40 m high, 100s of meters long	
Namibia[c]	igneous and metamorphic basement	8–0 km long; spacing 300–350 m	up to 20:1
Bolivia, Argentina, central Andes[g]	ignimbrite variably indurated, welded	100 m tall (indurated), 10 m tall (nonindurated); vertical to steep slopes	20:–40:1 (indurated), 5:1–10:1 (nonindurated)
Mars, MFF[h,i]	Medusa Fossae Formation	vertical to steep slopes; >100 m tall (range 5–700 m)	5:1 minimum to 20:1–50:1 maximum

[a] *McCauley et al.* [1977b].
[b] *McCauley* [1973].
[c] *Goudie* [2007].
[d] *Ward and Greeley* [1984].
[e] *Breed et al.* [1989].
[f] *Inbar and Risso* [2001].
[g] *Bailey et al.* [2007] and S. L. de Silva (manuscript in preparation, 2008).
[h] *Ward* [1979].
[i] This work.

considered to be viable at present: the deposits of pyroclastic flow or fall, and aeolian deposition.

[4] On Earth, deposits associated with these three processes are distinguished by characteristic material and deposit properties resulting from distinct depositional mechanisms and environments. For instance, although all might produce widespread sheet-like deposits that are generally fine-grained, pyroclastic flows of regional scale will inundate and bury topography and show variable jointing, induration, and welding [e.g., *Ross and Smith*, 1961; *Baker*, 1981; *Criswell and Elston*, 1981; *Selby et al.*, 1988; *de Silva*, 1989]. Moreover, while pyroclastic fall deposits and aeolian deposits may show small-scale induration and welding, they will not be pervasively indurated, welded, or jointed on a regional scale and will drape topography. Thus, through analogy with terrestrial deposits it should be possible in principle to distinguish between Martian pyroclastic flow deposits and those of fall origin such as ashfall or loess. The key then is to identify the deposit-wide characteristics of the MFF and what they reveal about its material properties.

[5] The apparent regional-scale consistency of the MFF material, fine-grain size, geologically young age, erosional features, and considerable vertical roughness (unevenness of the surface features derived from MOLA optical pulse width data), suggests that a dominant process likely produced most if not all of the deposit [*Scott and Tanaka*, 1982, 1986; *Greeley and Guest*, 1987]. Thus identifying the process that best explains the general characteristics of the MFF is one way of making some progress. Our approach has therefore been to take a synoptic perspective that focuses on characteristics that occur throughout the deposit because they represent the MFF as a whole. With this in mind, this contribution is based on the following three-pronged approach:

[6] 1. We have reviewed the available literature on the MFF and attempted to organize and classify all the disparate observations made about the MFF, and interpretations made thereof, into groups that inform about process (erosional or depositional), transport mechanism (aeolian, fluvial, glacial etc), and material properties (fine grained, indurated, jointed, friable). The entire analysis is summarized in Table 2, with further details in Table 3.

[7] 2. We have independently analyzed 713 Mars Orbiter Camera (MOC) images across the MFF to assess previous observations and to conduct our own synoptic survey of the deposit-wide characteristics (see auxiliary material).[1] This image analysis, combined with the literature review, allowed us to identify purely local versus deposit-wide characteristics.

[8] 3. We have evaluated the deposit-wide characteristics through a comparison with terrestrial analogs.

[9] Our main conclusions are that while yardangs, layering, and collapse features are found deposit wide, yardangs hold the most promise to inform about the origin of the MFF. These erosional features point to a process that produced friable regional-scale deposits that are layered, differentially indurated, and often jointed. The morphology of the yardang fields throughout the MFF is strongly analogous to those seen in terrestrial yardangs fields developed in extensive ignimbrites and may implicate a pyroclastic flow origin for much of the MFF.

[10] The MFF is located between two major volcanic centers. The eastern portion of the MFF is found on the upslope of the Tharsis rise while the western portion is located about 1000 km south of the Elysium volcanic center [*Scott and Tanaka*, 1986; *Greeley and Guest*, 1987]. The eastern portion of the MFF is partially overlain by a part of the "stealth region," an area of little to no radar signal

[1] Auxiliary materials are available in the HTML. doi:10.1029/2008JE003076.

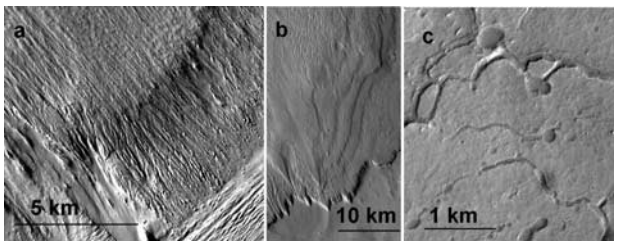

Figure 2. Erosional features of the MFF that were the focus of this study. (a) Portion of THEMIS visible image V19253002 centered at 177.4°E, 10.2°S, showing large-scale yardangs in the MFF. (b) Portion of THEMIS daytime IR image I01280001 centered at 189°E, 7.24°S, showing layered terrain in the MFF. (c) Portion of MOC image E03-01084 centered at 178.8°E, 2.2°N, showing collapse features in the MFF.

thought to be lightweight material of volcanic origin [*Edgett et al.*, 1997]. In all places where they are in contact, the southern portion of the MFF overlies the hemispheric dichotomy boundary [*Scott and Tanaka*, 1986; *Greeley and Guest*, 1987; *Bradley et al.*, 2000; *Head and Kreslavsky*, 2001, 2004; *Hynek et al.*, 2003]. The MFF has been divided into three members (upper, middle, and lower) on the basis of morphology, stratigraphy, albedo and apparent age [*Scott and Tanaka*, 1986; *Greeley and Guest*, 1987]. Though reevaluation of this mapping was advised when early Mars Orbiter Laser Altimeter data was analyzed [*Sakimoto et al.*, 1999], a deposit-wide reevaluation has not yet been published. Though the MFF stretches for over 5000 km and covers an elevation range from −2000 to +2000 m, it is not continuous over that distance, but broken up into segments of 1000–2000 km, separated by up to 1000 km in the western portion of the deposit. Albedo varies from low to high within the deposit [*Scott and Tanaka*, 1982] and boulders are not seen at erosional contacts [*Malin and Edgett*, 2000; *Hynek et al.*, 2003].

3. Analysis of the Literature

[11] During an exhaustive review of the literature we have found that over one hundred separate observations have been used to support the conclusions of 33 published studies of the MFF (Table 2). We have classified these observations into *extrinsic*, those that inform about process (transport, emplacement, erosion) and *intrinsic*, those that inform about the lithology, morphology, and material properties of the deposit. Examples of the former are bedding [*Malin and Edgett*, 2000] that implies an intermittent accumulation, as well as draping [*Bradley and Sakimoto*, 2001] and an apparent thickening toward Tharsis [*Hynek et al.*, 2002, 2003] that have been used to suggest a pyroclastic fall origin. Intrinsic attributes include raised curvilinear features [*Burr et al.*, 2006], stair steps [*Malin and Edgett*, 2000], knobs [*Scott and Tanaka*, 1982; *Schultz and Lutz*, 1988; *Bradley and Sakimoto*, 2001; *Nussbaumer et al.*, 2003; *Nussbaumer*, 2005], and yardangs [*Scott and Tanaka*, 1982; *Bradley et al.*, 2002]; these all speak to the nature of the MFF material.

[12] Our complete analysis of the literature on the MFF is given in Table 2. It is clear from this literature review that a strong consensus is shown for the following attributes of the MFF:

[13] 1. Large aerial extent ($2.1–2.5 \times 10^6$ km^2) and volume ($1–1.9 \times 10^6$ km^3) [*Scott and Tanaka*, 1982; *Tanaka*, 2000; *Bradley et al.*, 2002; *Head and Kreslavsky*, 2001, 2004; *Hynek et al.*, 2003].

[14] 2. Amazonian age is based on the following evidence. The upper member of the MFF overlies the youngest aureole deposits [*Head and Kreslavsky*, 2001], though interweaving with some younger lava flows has been observed where the MFF borders the Cerberus Plains [*Lanagan and McEwen*, 2003]. Otherwise, the MFF appears to overlie all other geologic formations in its region. These stratigraphic relations have determined that most of the MFF was emplaced in the Amazonian Period [*Scott and Tanaka*, 1982, 1986; *Greeley and Guest*, 1987; *Bradley and Sakimoto*, 2001; *Head and Kreslavsky*, 2001, 2004; *Hynek et al.*, 2003]. *Head and Kreslavsky* [2001, 2004] suggest that the complex stratigraphy described above indicates that deposition may have begun as early as the Hesperian.

[15] 3. Multiple episodes of deposition as evidenced by changing yardang orientations [*Scott and Tanaka*, 1982; *Bradley and Sakimoto*, 2001; *Hynek et al.*, 2002, 2003], complex stratigraphy [*Head and Kreslavsky*, 2001, 2004], and craters between layers [*Tanaka and Leonard*, 1998, *Sakimoto et al.*, 1999; *Hynek et al.*, 2002, 2003].

[16] 4. Fine-grain size based on the lack of boulders along erosional contacts [*Malin and Edgett*, 2000; *Hynek et al.*, 2003], different crater depth-diameter ratios than areas known to be caprock [*Barlow*, 1993], erosional morphology (yardangs, chutes or dark scree slopes and pedestal craters) [*Hynek et al.*, 2003; *Malin and Edgett*, 2000; *Schultz and Lutz*, 1988], low thermal inertia and radar signals [*Hynek et al.*, 2003].

[17] 5. Heavily eroded by aeolian processes [*Bradley et al.*, 2002; *Head and Kreslavsky*, 2001, 2004; *Hynek et al.*, 2003; *Malin et al.*, 1998; *Zimbelman et al.*, 1997a; *Greeley and Guest*, 1987; *Scott and Tanaka*, 1986; *Frey et al.*, 1998; *Takagi and Zimbelman*, 2001; *Schultz and Lutz*, 1988] with an estimated original aerial extent of 5×10^6 km^2 [*Bradley et al.*, 2002].

[18] Beyond this, our analysis has also allowed us to eliminate specific local features such as draping [see also *Watters et al.*, 2007], and has resulted in the identification of a set of deposit-wide features that have been ubiquitous in studies of the MFF: yardangs, collapse features, and layering (Figure 2). The yardangs hold the most promise for providing insight into material properties. The collapse features and layering are seen deposit wide, but are equivocal and will require more investigation with higher-resolution data to be useful.

3.1. Yardangs

[19] Yardangs are aerodynamically shaped landforms that represent the remnants of deposits eroded by the wind and are the most commonly observed features in the MFF [*Ward*, 1979]. They occur across the extent of the deposit and within various members at different elevations. Though most publications refer to the yardangs, few provide detail on their texture or appearance. Focus has primarily been on their wide variety of orientations [*Scott and Tanaka*, 1982; *Zimbelman and Patel*, 1998; *Zimbelman et al.*, 2000;

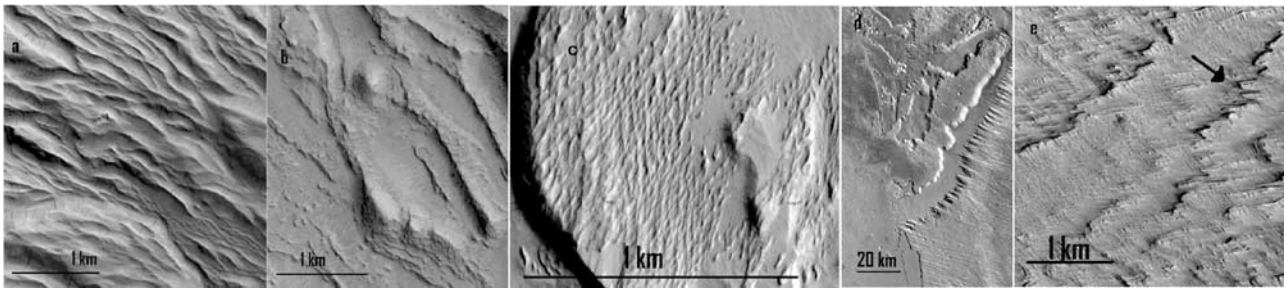

Figure 3. Examples of MFF yardang characteristics. (a) Portion of MOC E10-03225, centered at 221.1°E, 4.27°S, showing smooth-textured curvilinear yardangs. (b) Portion of MOC M09-04901 centered at 147.37°E, 6.45°S, showing rough-textured curvilinear yardangs. (c) Portion of MOC M08-01561 centered at 7.42°N, 197.11°E, showing bidirectional yardangs and an exhumed crater. (d) Portion of THEMIS infrared I17167016 centered at 209.742°E, 2.241°N, showing a large-scale example of a serrated or feathered scarp. Scarp is 3 km high. (e) Portion of MOC E04-00932 centered at 210.63°E, 3.7°N, with arrow pointing to a small-scale example of the serrated or feathered scarp.

Bradley et al., 2002; *Hynek et al.*, 2003; *Zimbelman*, 2003] and their proof of extensive aeolian erosion. All members of the MFF display yardangs, so they are clearly a formation-wide characteristic. Two studies have focused on yardangs formed in MFF material.

[20] *Ward* [1979] observed that Martian yardangs had aspect ratios (length:width) up to 50:1 and suggested that they are much larger than those known on Earth, and they. He suggested this to be the result of a lack of secondary processes (e.g., fluvial erosion) to subdue their forms, thicker formations on Mars than on Earth, and that trough extension was much faster than streamlining. He suggested that the lithology of the MFF had to be something that weathered to a granular substance that could be efficiently deflated.

[21] *Bradley et al.* [2002] observed bidirectional yardangs in 23% of the 155 MOC Narrow Angle images available at the time of their survey of the MFF. They interpreted the consistent angle of intersection (Figure 3c) to be a sign of columnar jointing, which is in agreement with other researchers [*Scott and Tanaka*, 1982, 1986; *Zimbelman et al.*, 1997b]. *Bradley et al.* [2002] posited that this apparent jointing was developed through cooling and compaction on the basis of terrestrial analog studies. They noted that joint patterns are not found throughout the entire MFF, and suggest that this is either due to wind direction being the dominant force on yardang orientation, or because jointing is not found throughout the formation.

3.2. Collapse Features

[22] In a study of the middle member of the MFF located between 180 and 192°E (168–180°W) longitude and 2°N–4°S latitude, *McColley et al.* [2005] noted several kilometer-scale rectilinear troughs (see Figure 2c). They interpreted these depressions to be created by subsurface collapse or movement on scales ranging from one to tens of kilometers, and to be the result of volatile release. On the basis of the literature these features appear to be local, but the image analysis described in the next section shows otherwise. Similar features have been observed elsewhere on Mars, but generally on a much larger scale (observable in THEMIS (Thermal Emission Imaging System) images) and with a more linear appearance. The frequency of these features in areas showing regional extension or local fissuring led to their interpretation to be the result of dilational faulting [*Wyrick et al.*, 2004].

3.3. Layering

[23] Many authors have observed signs of layering throughout the deposit [*Scott and Tanaka*, 1982, 1986; *Zimbelman et al.*, 1997a; *Zimbelman and Patel*, 1998; *Forsythe and Zimbelman*, 1988; *Sakimoto et al.*, 1999; *Malin and Edgett*, 2000; *Bradley and Sakimoto*, 2001; *Bradley et al.*, 2002; *Hynek et al.*, 2003], although only a few provide specific details characterizing the layering. Three layers at the scale of hundreds of meters were observed in MFF material in the region of the Gordii Dorsum [*Zimbelman et al.*, 1996; *Zimbelman and Patel*, 1998]. Hundreds of meter-scale layers were observed using MOLA data near Apollineras Patera and south of Elysium Mons [*Bradley et al.*, 2002]. Layering at the scale of 10s of meters cannot be observed using MOLA data, but some evidence of such layering was seen in the 2002 survey of 155 MOC images [*Bradley et al.*, 2002]. The area of the layering is uncertain from the literature.

4. Image Analysis

[24] We have examined 713 MOC Narrow Angle (1.5–3 m per pixel for the images surveyed) images of the MFF (Figure 4) that were obtained from the NASA Planetary Data System at http://ida.wr.usgs.gov/. Each

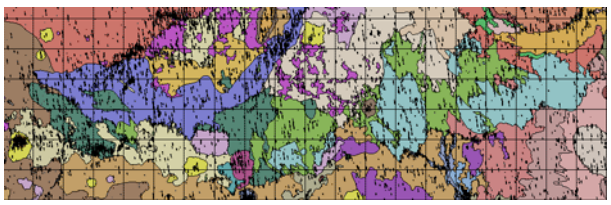

Figure 4. Footprints of MOC images overlain on a portion of the Viking-based geologic map of Mars showing the MFF [*Scott and Tanaka*, 1986; *Greeley and Guest*, 1987]. Map range is −15 to +15°N latitude and 135–245°W longitude with 5° grid spacing. The MFF units are shown in dark green, light green, and teal.

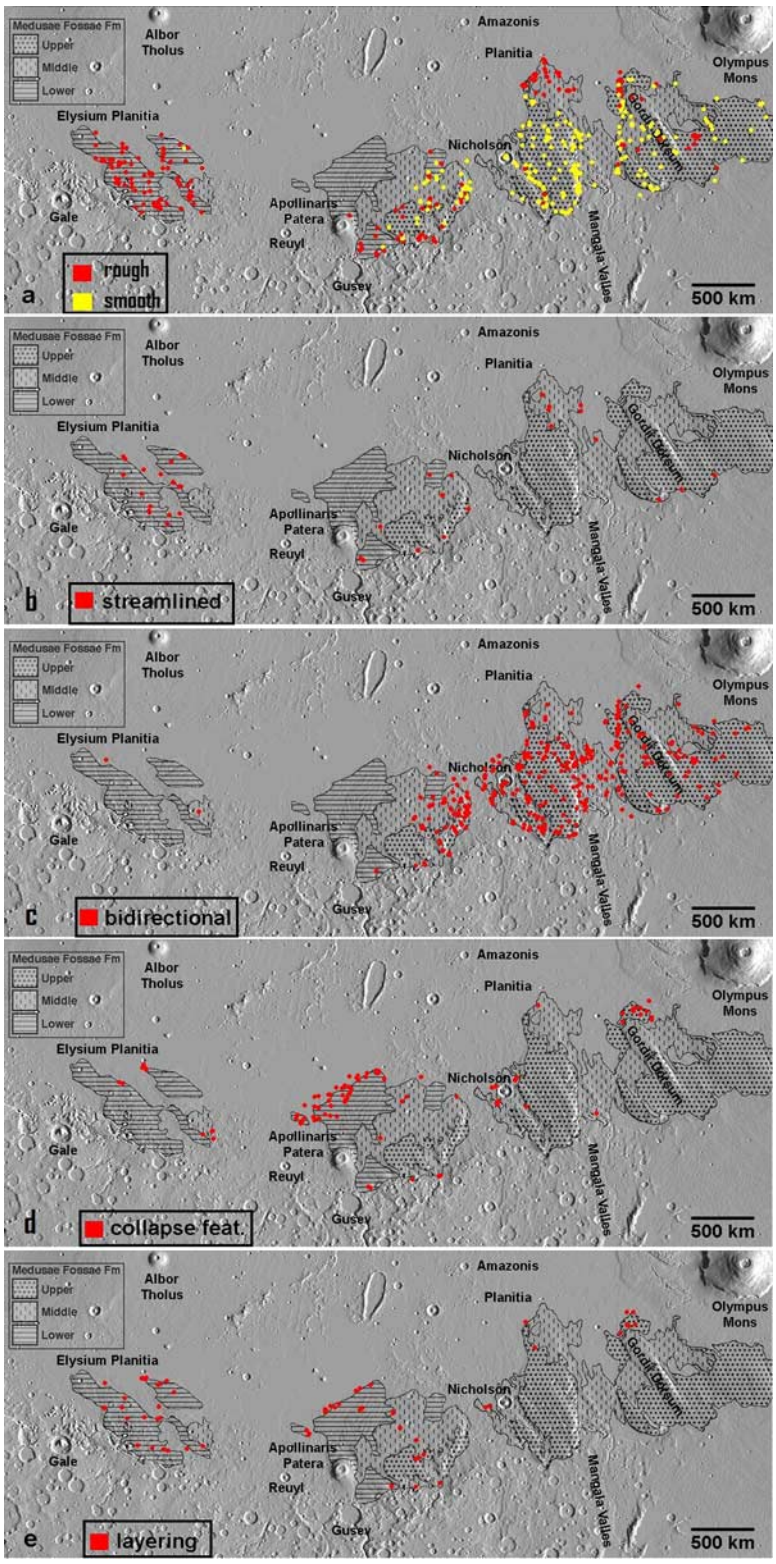

Figure 5. (a) Locations of MOC images showing rough and smooth-textured curvilinear yardangs. (b) Locations of MOC images showing streamlined yardangs. (c) Locations of MOC images showing bidirectional yardangs like those seen in Figure 2c. (d) Locations of MOC images showing erosional patterns interpreted as collapse features. (e) Locations of MOC images showing layering at the scale of 10s of meters.

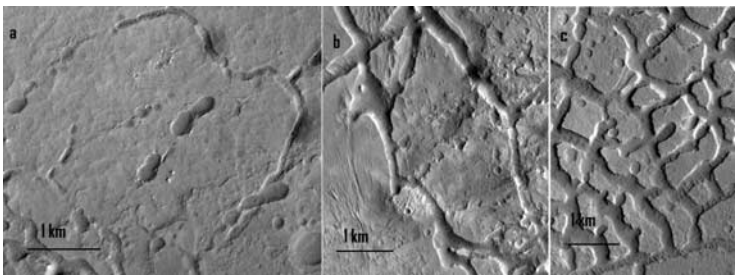

Figure 6. Examples of characteristics of collapse features. (a) Portion of MOC E03-01084 centered at 178.8°E, 2.2°N, showing collapse pits in center with troughs on the perimeter. (b) Portion of MOC E05-02396 centered at 178.14°E, 2.31°N, showing troughs formed from collapse pits. (c) Portion of MOC R04-02077 centered at 172.85°E, 1.68°S, showing geometric pattern commonly seen in MFF collapse troughs.

individual image was analyzed in conjunction with the Mars Spaceflight Facility at Arizona State University's online Geographical Information System (GIS): Java Mission Planning and Analysis for Remote Sensing (JMARS) http://jmars.asu.edu [*Christensen et al.*, 2007]. The JMARS day and night global THEMIS layers were used to provide medium resolution (230 m/pixel) context for the MOC images. Additionally, the JMARS MOLA 16-bit elevation data, at 128 pixels/°, were used to create topographic profiles to evaluate large-scale layering, and heights and slopes of the larger MFF yardangs. Our observations focused on the three main features we have identified as characteristic of the MFF as a whole: yardangs, collapse features and layering. The footprints of each image in our database (available as a digital addendum to this paper) containing these features are shown in Figure 4.

4.1. Yardangs

[25] Yardangs occur as extensive fields, some with areas of up to 40,000 km^2, and are clearly visible at THEMIS resolution. Of the 713 MOC images of MFF, 78% showed yardangs in some form.

[26] Two types of yardang shape were seen in the MOC images: curvilinear, characterized by curving lines or edges (55% of all images surveyed) and streamlined, having a smooth even shape (6% of all images surveyed). The MFF yardangs are predominantly curvilinear in form. The texture of these yardangs ranges from smooth surfaced (Figure 3a) to rough, with a platy or sharp-edged appearance (Figure 3b). 54% of the curvilinear yardang images were smooth and the remainder rough. The locations of images showing these yardangs are mapped in Figure 5a, indicating that yardangs with similar textures tend to be grouped together. Smooth yardangs appear to be more common in the middle and upper members whereas rough yardangs are more common in the middle and lower members. Aspect ratios (length:width) of the curvilinear yardangs range from 5:1 to 20:1, but there is no clear trend between aspect ratio and texture or spatial distribution. Streamlined yardangs (Figure 3c) appear to be relatively rare in the MFF (mapped in Figure 5b). They also coincide with areas where curvilinear yardangs are common. The aspect ratios of the streamlined yardangs seen in 40 MOC images range from 3:1 to as high as 50:1.

[27] Bidirectional yardangs (Figure 3c) appear to trend in two directions with an angle of intersection between 30 and 45° [*Bradley et al.*, 2002]. These yardangs are only about 10–15 m wide and 30–40 m long and are seen in 44% of the MOC images surveyed (mapped in Figure 5c). They are too small to be seen at THEMIS resolution, and MOC resolution is insufficient to discern clearly the shape or texture of these yardangs. Of the 713 images, 554 showed yardangs in some form: 204 curvilinear only, 125 bidirectional only, 186 curvilinear and bidirectional, 31 streamlined, 8 streamlined and bidirectional. Of the images showing both curvilinear and bidirectional yardangs, 157 (84%) have smooth curvilinear yardangs suggesting a strong relationship between the smooth curvilinear and bidirectional yardangs.

4.2. Collapse Features

[28] We have found features that resemble the pit chains and rectilinear troughs observed by *McColley et al.* [2005] and *Wyrick et al.* [2004] in 14% of the MOC images surveyed (mapped in Figure 5d). They are not as prevalent in the MFF as the yardangs, but they are seen in all geographic areas and all three members of the formation. The majority of these features are seen at the edges of the deposit where relief is limited to less than 250 m.

[29] The pits that the chains and troughs form from (Figure 6a) are about 50–100 m in diameter and are circular or elongate in shape. Troughs range from 100 to 250 m wide and can extend several kilometers in length (Figure 6b). The troughs form in many different directions and intersect at a variety of angles, creating varied geometric patterns in the MFF material (Figure 6c).

4.3. Layering

[30] We have found very limited evidence for layering in the MFF at the scale of 100s of meters beyond the evidence cited by previous workers. Only five MOC images showed cliffs greater than 400 m high with benches resulting from probable layers in the cliffs (Figure 7a). Moreover, the MOLA shot size on Mars is ~160 m and the shot spacing is typically ~330 m (endnote 12 of *Smith et al.* [1999]), which limits the ability to discern layering at this scale.

[31] Features that appear to represent layering at a scale of 10s of meters can be noted in some MOC images with caprock layers over friable material and "onion skin" topography (Figures 7b and 7c), which is a common aeolian erosional feature found in terrestrial material with layering

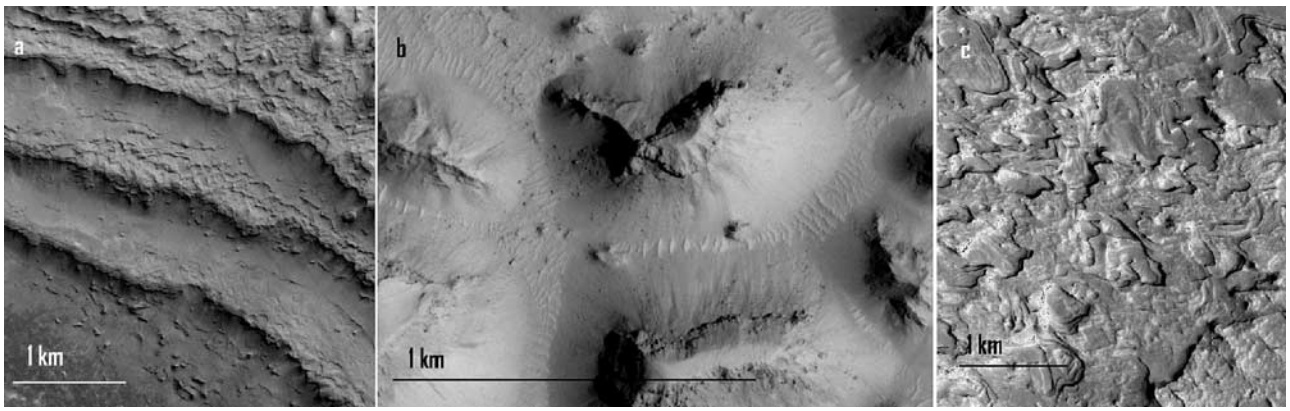

Figure 7. Examples of features that characterize layering in the MFF. (a) Portion of MOC M12-02293 centered at 148.95°E, 2.79°S, showing three distinct benches in a 600 m high cliff. Illumination is from top. (b) Portion of MOC E05-01356 centered at 147.45°E, 3.32°N, showing a layer of caprock breaking off as the less indurated layer below is eroded. (c) Portion of MOC M02-02978 centered at 142.09°E, 0.25°S, showing an example of onion skin topography.

at this scale. Figure 5e shows the locations of MOC images which evidence layering.

[32] The layering is present in each of the mapped members of the formation so it could be described as formation wide, but is not abundant enough to be described as extensive. At this stage we cannot determine whether the observed layering represents primary bedding, grading, a superimposed property such as differential welding or induration or some combination of these. Higher-resolution data (e.g., HiRISE) will play an important role in further defining the character of layering in the MFF.

5. Discussion

[33] In an attempt to resolve between the three most likely origins for the MFF, we have taken a synoptic view of the formation and tried to identify the deposit-wide characteristics as a means of addressing the origin of the formation as a whole.

[34] As recognized by previous workers, the MFF is a deposit of large aerial extent and volume that shows certain deposit-wide characteristics like its young (Amazonian) age, evidence for multiple episodes of deposition, a pervasively fine-grained nature, and erosion by aeolian processes. However, these general characteristics alone do not inform about a specific process of origin and our effort has been to try and identify features in the MFF that are a function of the deposit properties, as we believe these will vary as a function of depositional mechanism. For instance, by analogy with Earth, deposition by pyroclastic flows will result in induration and welding characteristics and cooling and compaction related to jointing and fracturing that are not typical of primary fall or aeolian deposits. Welding in ashfall deposits is local and limited to less than 10 km from the source [e.g., *Cas and Wright*, 1992], and these are otherwise completely friable, as is loess directly after deposition. Any induration process for air fall deposits on the surface of Mars would be secondary and is therefore another degree removed from a primary mechanism. Given the large area of the MFF and our focus on deposit-wide characteristics, it is difficult to envision a consistent and pervasive deposit-wide induration process that could take place under Amazonian conditions that is not linked to its formation. The properties of deposits from these three mechanisms (pyroclastic flow, pyroclastic fall and loess) should therefore be quite distinct.

[35] Our analysis has identified three features that are characteristic of the MFF across its extent; yardangs, collapse features, and layering. Of these three, we find that collapse features and layering do not provide enough information at this time to allow us to differentiate between the viable hypotheses of origin of the MFF materials; layering could result from any of the three processes, and the resolution of the data is insufficient to differentiate between styles of layering. In turn, collapse features are enigmatic. Surface erosion alone cannot fully explain the collapse features, so some sort of subsurface activity must be involved in their formation. Whether this is due to volatile release [*McColley et al.*, 2005], faulting [*Wyrick et al.*, 2004] or some other process is difficult to discern at this time.

[36] Ultimately, the yardangs appear to hold the most promise for inferences regarding formation. The form and texture of wind-eroded forms is strongly dependant on rock structure and lithology because these control the erosional effectiveness of the wind [*Breed et al.*, 1989] and the character of the ridges and slopes of the forms [*Selby et al.*, 1988]. On Earth, extensive yardang fields are found in a variety of deposits ranging from lake deposits (Iran), sandstones (Peru), and ignimbrites and lava flows (Andes), among others, as summarized in Table 3. This compilation shows that although there is wide-ranging variability in yardang morphology, there is a strong relationship between aspect ratio, height, and slopes. These are largely a function of the degree of induration of the deposits, with poorly indurated material forming small, stubby yardangs, and indurated deposits supporting long, high, steep-sided yardangs. This discussion now focuses on the properties of yardangs and their implications for the origin of the MFF.

5.1. Yardangs in the MFF

[37] *Ward* [1979] observed that yardangs in the MFF on Mars were considerably larger and more elongate (aspect ratios up to 50:1) than mature terrestrial yardangs (aspect ratio 4:1 [*Ward and Greeley*, 1984]). He suggested that the

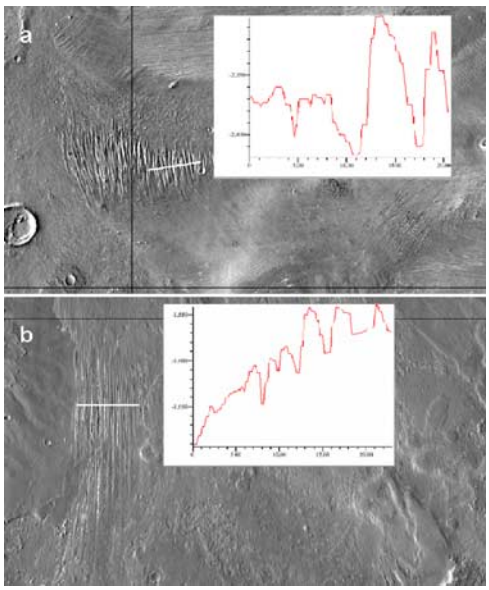

Figure 8. Examples of topographic profiles derived from MOLA 128 pixels/° DEM, created using JMARS to evaluate the height, width, and slope of large-scale yardangs. (a) Yardangs in the western portion of the MFF formed along a steep slope facing into the inferred primary wind direction on the basis of yardang orientation [*McCauley et al.*, 1977a]. The profile line is centered at 150.28°E, 0.79°N. (b) Yardangs in the central portion of the MFF. In this case the topographic slope is perpendicular to the wind that formed the yardangs, so the yardangs formed perpendicular to the slope. The profile line is centered at 176.64°E, 10.57°S.

size, slopes, and forms of Martian yardangs implied an indurated lithology that weathers to a granular substrate. The other pervasive lithologic property attributed to the MFF lithology is jointing, which *Bradley et al.* [2002] attributed to cooling and compaction [see also *Scott and Tanaka*, 1982].

[38] We have attempted to further these analyses by establishing more detailed morphometric parameters for the MFF yardangs. The height and slope of yardangs that are wider than one kilometer can be evaluated with the MOLA topographic profile tool in JMARS (Figure 8). Although these megayardangs only represent about 7% of the aerial coverage of the yardangs in the formation, this analysis gives some insight into these particular yardangs. The slopes of these megayardangs are on average 75–80° and they range in height from 5 to 700 m, with the majority being over 100 m tall (Figure 8). Their width ranges from one to five kilometers. Aspect ratios (length:width) vary widely but can be greater than 50:1, with yardangs that are several tens of kilometers long. Because slope, height and aspect ratio are largely a function of the degree of induration of the deposits, these measurements suggest heavily indurated material.

5.2. Inferred Material Properties of the MFF and a Likely Analog Lithology

[39] Our analysis of the MFF is consistent with a layered lithology that supports a range of yardang morphologies and develops jointing. At one extreme, the steep slopes and height of the megayardang ridges in the MFF point to a strong lithology, as the ability to support such forms is a characteristic of strong rocks [*Selby et al.*, 1988]. However, the variable size, forms and textures of yardangs seen at high resolution suggest that some are made from weaker materials. The material must weather to a granular substance that is easily deflated by the wind [*Ward*, 1979]. By analogy with Earth, these properties suggest variably cemented or indurated deposits of clastic material, either sediments or pyroclastic rocks. The potential presence of jointing is important. Direct evidence for jointing is difficult to find, and we note that *Bradley et al.* [2002] largely inferred this to explain bidirectional yardangs. We note that some of the MFF yardang fields form perpendicular to a scarp or slope greater than 45°, leaving a serrated edge in the scarp or feathering of the slope (Figures 3d and 3e). The images showing streamlined forms are among areas with abundant curvilinear yardangs, so it is likely that these were originally curvilinear in form and eroded into more streamlined features. Thus we interpret no difference between the lithology of the different yardang types.

[40] Of the potential analogs for the MFF on Earth, neither volcanic air fall deposits nor loess (suspended silt) deposits display characteristics consistent with the MFF. These deposits are rarely indurated or jointed on a regional scale. Ancient loess deposits on Earth (Paleozoic) may be indurated and behave as strong rocks after burial and metamorphism [e.g., *Tramp et al.*, 2004] but young loess deposits are rarely consolidated and behave as weak to strong soils once subjected to surface pedogenesis [*Günster et al.*, 2001]. These deposits collapse as granular flows as during the 1556 Shaanxi Earthquake [*People's Republic of China*, 1982, p.100]. No examples of regional extensive indurated pyroclastic fall deposits are known to the authors. We also do not know of extensive yardang fields that have developed in these deposits. Thus, if pyroclastic fall and/or loess deposits form the MFF, induration would have to be the result of secondary processes. It would likely be a low temperature hydrous/chemical process like that seen in loess deposits [*Günster et al.*, 2001] but would have to work from the top down to give the strength profile required (top stronger than bottom inferred from the discontinuous but pervasive layering characteristics observed at high resolution). Such induration processes are rarely pervasive, typically produce only incipient induration and do not produce systematic jointing on a large scale.

[41] On the contrary, ignimbrites, the depositional product of pyroclastic flows, display the range of characteristics that have been attributed to the MFF. In fact of all the terrestrial yardang fields examined by us (Table 3), the erosional pattern is most pervasive where ignimbrites are the host lithology. Ignimbrites, uniquely in our opinion, develop the range of properties found in the MFF because of their depositional environment, and we show below that this is probably the most likely lithology in the MFF.

5.3. Yardangs in Terrestrial Ignimbrites

[42] As part of an ongoing study of extensive ignimbrites of the Central Andes [*de Silva*, 1989; *de Silva et al.*, 2006], we have found that a wide range of yardang morphologies is produced by the variable material properties that characterize

extensive regional ignimbrite sheets. The ignimbrites of the Central Andes are among the largest on Earth, with volumes in excess of 1000 km^3 and areas of over 10,000 km^2. At the scale of remotely sensed data, layering can be distinct in plateaus consisting of several stacked sheets, but can also be found within individual sheets, although this is rarely pervasive. Ignimbrites are fragmental (volcaniclastic) rocks, and large ignimbrites like these typically show two main facies: an upper massive, indurated and jointed facies, the result of postdepositional induration by escaping heat and hot gasses [*Roever*, 1966; *de Silva*, 1989] and a lower weak to poorly indurated, massive ash- and pumice-rich facies (Figure 9 (top)). These facies have a welding profile superimposed on them, but this is not typical and is only local in occurrence. The two main facies may occur individually, and may be locally vertically associated, or regionally grade into each other laterally (the result of heat loss by the pyroclastic flow as it travels). The two facies have quite different mechanical properties; the upper facies behaves as strong rock, fails by block collapse and supports steep/vertical cliffs, whereas the lower facies has deeply weathered soils and forms gentle slopes [*Selby et al.*, 1988; *Crown et al.*, 1989]. These two facies produce yardangs of quite different character (Figure 9). The presence of the indurated facies results in massive, extremely elongate, high aspect ratio (20:1 to 40:1) yardangs, that form tall (100 m), thin ridges with steep to vertical walls (Figure 9 (top and middle)). This type of yardang demonstrates the importance of differential induration and mechanical weathering in producing tall, steep-sided, megayardangs with broad shallow-sloped bases. Weakly indurated ignimbrites are carved into stubby and chaotic yardangs with aspect ratios of 5:1 to 10:1 and heights rarely exceeding 20 m (Figure 9 (bottom)). The indurated (not necessarily welded) facies is commonly pervasively jointed [*de Silva*, 1989], and the development of yardangs in these areas clearly demonstrates that a persistent, strong unidirectional wind is the dominant parameter controlling yardang orientation [*Inbar and Risso*, 2001; *Bailey et al.*, 2007]. In many locations, we have found serrated margins quite like those in the MFF to be the result of oblique intersections of jointing and yardangs or scarps of ignimbrite sheets (Figure 10).

[43] We suggest that these terrestrial ignimbrites provide the strongest analog to much of the MFF and we concur with previous workers such as *Scott and Tanaka* [1982, 1986] that a large part of the MFF resulted from the deposition by pyroclastic flows. If so, it is interesting to speculate about possible source structures for these massive eruptions. Studies of Martian plume stability suggest that pyroclastic flows could extend for hundreds of kilometers from the source [*Wilson and Head*, 1994], though *Glaze and Baloga* [2002] set limits on eruption conditions that would allow flows up to only 200 km from the source. Previous analyses of the energetics of explosive volcanic eruptions in conjunction with the Martian highland paterae suggested that their flanks lengths (e.g., over 400 km for Hadriaca Patera) were too great to result from air fall deposits (given required eruption column heights) and attributed the formation of Hadriaca and Tyrrhena Paterae to pyroclastic flow emplacement driven by either magmatic or hydromagmatic explosive eruptions [*Greeley and Crown*, 1990; *Crown and Greeley*, 1993]. Models of cooling during

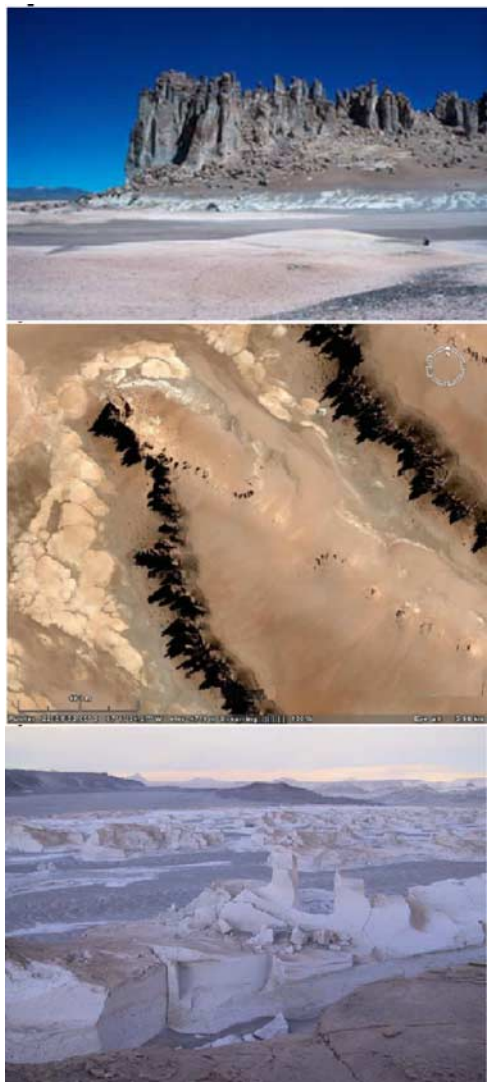

Figure 9. Yardangs in ignimbrites in the central Andes. (top) Megayardang in the 3.6 Ma Tara ignimbrite plateau in northern Chile. Wind is from the left. The yardang is 100 m tall and consists of a white poorly indurated base forming a shallow sloped platform to the vertical walled "blade" of the vapor phase indurated facies. (middle) Aerial view of the same yardang used with permission of Google Earth imagery © Google Inc., map data copyright 2007 DMapas/El Mercamio, and image copyright 2007 DigitalGlobe. Note the columnar structure of the blade produced by pervasive jointing in the indurated facies and formation of an extensive block field at the base resulting from collapse. This yardang demonstrates the importance of differential induration and mechanical weathering in producing tall, steep-sided, megayardangs with broad shallow sloped bases. Image centered at 22°51′43.15″S, 67°18′09.59″W. (bottom) Aeolian erosion of the poorly indurated Campo Piedra Pomez ignimbrite (~70,000 years old) in the Puna of Argentina. Elevation is ~4000 m. Yardangs are relatively small ranging up to 20 m high and 100 m long, with aspect ratios of 5:1–10:1. Note weak layering within the ignimbrite seen in the foreground. There are no massive vertical walls and tall feature is minimized through block collapse. Gravel ripples and dunes are found in the troughs. Wind direction is from the right.

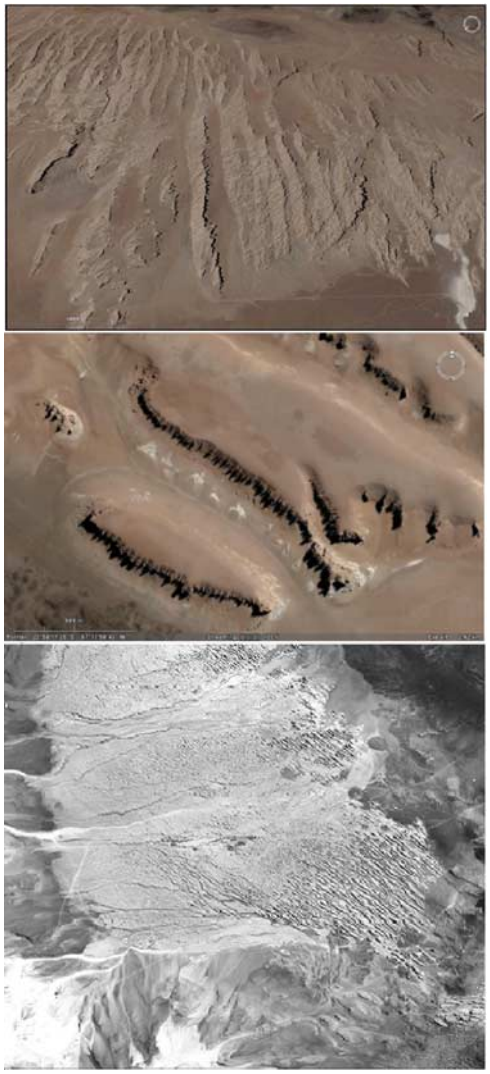

Figure 10. Formation of a serrated scarp. (top) Aeolian erosion and yardang formation in the indurated 5.6 Ma Chuhuihuilla ignimbrite in southwest Bolivia. Oblique view from west to east used with permission of Google Earth imagery © Google Inc. and image copyright 2007 TerraMetrics. Prevailing wind is from NW to SE. The longest of these ridges is about 2 km long and aspect ratios of 20:1 are common here. Note the discordance between pervasive jointing and wind direction producing serrated margins and rhomboid blocks. (middle) Serrated edges in mature yardangs (aspect ratio 4:1) in the 3.6 Ma Tara ignimbrite produced by pervasive jointing oblique to wind direction (from right). The yardangs have grown by deepening and widening ancestral fluvial channels. Image used with permission of Google Earth imagery © Google Inc. and image copyright 2007 DigitalGlobe. Image center: 22°58′11″S 67°17′58″W. (bottom) Portion of aerial photo 22,1378 (15 April 1961) of Cerro Escorial region in Argentina (10 km across). North is to the top. Prevailing wind direction is NW-SE (from top left to bottom right), but local channeling by topography produces a weak sinuosity to the yardang orientation. Several stages of yardang formation and surface erosion can be seen from incipient, mature through to stripped. Aspect ratios vary from 4:1 to about 10:1. Serrated edges are seen where fluvial erosion exposes jointing in ignimbrite.

emplacement indicate that welding within pyroclastic flows could occur at large distances from a source vent on Mars and thus could explain layering within extensive volcanic deposits [*Crown and Greeley*, 1993]. Given the limits on the distribution of volcanic materials, multiple local sources within and buried by the deposit are necessary for either type of deposit. *Scott and Tanaka* [1982] identified three collapse features to be possible source vents, and *Tanaka* [2000] suggested that the Gordii and Eumenides Dorsa and an unnamed dorsum, all located in areas of 1–3 km relief, were possible source fissures. Eruption of major ignimbrites from fissures, faults or volcano-tectonic features is increasingly being recognized on Earth [*Aguirre-Diaz and Labarthe-Hernandez*, 2003; *de Silva et al.*, 2006] and may explain the lack of evidence for distinct "caldera" structures that could have sourced the MFF.

6. Conclusion

[44] Researchers are in agreement about some characteristics of the MFF such as its young (Amazonian) age, the evidence for multiple episodes of deposition, its pervasively fine-grained nature, and the evidence for heavy erosion by aeolian processes. However, none of these characteristics can discriminate between the three viable origins for the MFF; pyroclastic flow, pyroclastic fall and aeolian (loess). A survey of MOC Narrow Angle images identified three features that are seen deposit wide: yardangs, collapse features, and layering. The collapse features are in themselves enigmatic but suggest some postdepositional processes and need further investigation before they can inform about the origin or material properties of the deposit. The evidence for layering is not abundant, but occurs in all geographic areas of the MFF. Higher-resolution data can better characterize the layering to provide insight into origin. Yardangs provide the greatest insight into material properties of the MFF. With aspect ratios of up to 50:1 and nearly vertical cliffs, yardangs in the MFF suggest a lithology that displays a wide range of induration, in some areas strong enough to support steep cliffs. Jointing is inferred from the bidirectional yardangs and the serrated margins, but requires higher-resolution data to test directly.

[45] The similarity of the morphological features displayed by the MFF yardangs and those of the terrestrial ignimbrites is striking. The depositional processes and resulting lithologic characteristics of large ignimbrites in the Central Andes provide the most viable analog to the MFF lithology. We recognize that large terrestrial ignimbrites are typically felsic in composition, and that large-scale silicic volcanism is not known on Mars [*Francis and Wood*, 1982]; however, we note that basaltic ignimbrites on Earth, although considerably smaller in volume, do display similar facies variations [*Freundt and Schmincke*, 1995; *Giordano et al.*, 2006]. We would anticipate that pyroclastic eruptions on Mars, even if they are mafic, would produce deposits with a similar range of facies and therefore display physical properties similar to the large terrestrial ignimbrites discussed here. An ignimbrite is the only hypothesis presented to date that explains all of the major observations with a single mechanism.

[46] **Acknowledgments.** K.M. acknowledges research support from a 2006 North Dakota View Consortium Grant. S.D.S. thanks North Dakota NASA Space Grant and Oregon NASA Space Grant Consortium for support to conduct some of this work. Portions of this work were supported by NASA PGG grant NNX07AP42G to J.R.Z. for the investigation of MFF. The detailed review by an anonymous reviewer and the editorial handling by Robert Carlson improved the form and content of this paper considerably and are gratefully acknowledged.

References

Aguirre-Diaz, G. J., and G. Labarthe-Hernandez (2003), Fissure ignimbrites: Fissure-source origin for voluminous ignimbrites of the Sierra Madre Occidental and its relationship to basin and range faulting, *Geology*, *31*(9), 773–776, doi:10.1130/G19665.1.

Bailey, J. E., S. Self, L. K. Wooller, and P. J. Mouginis-Mark (2007), Discrimination of fluvial and eolian features on large ignimbrite sheets around La Pacana Caldera, Chile, using Landsat and SRTM-derived DEM, *Remote Sens. Environ.*, *108*(1), 24–41, doi:10.1016/j.rse.2006.10.018.

Baker, M. C. W. (1981), The nature and distribution of upper Cenozoic ignimbrite centres in the Central Andes, *J. Volcanol. Geotherm. Res.*, *11*, 293–315.

Barlow, N. G. (1993), Increased depth diameter ratios in the Medusae Fossae Formation deposits of Mars (abstract), *Proc. Lunar Planet. Sci. Conf.*, *24*, 61–62.

Bradley, B. A., and S. E. H. Sakimoto (2001), Relationships between the Medusae Fossae Formation (MFF), fluvial channels, and the dichotomy boundary southeast of Nicholson Crater, Mars (abstract), *Proc. Lunar Planet. Sci. Conf.*, *32*, 1335.

Bradley, B. A., E. B. Grosfils, and S. E. H. Sakimoto (2000), Boundaries of the Medusae Fossae Formation and Elysium Basin materials using Mars Orbiter Laser Altimeter (MOLA) data (abstract), *Proc. Lunar Planet. Sci. Conf.*, *31*, 2055.

Bradley, B. A., S. E. H. Sakimoto, H. Frey, and J. R. Zimbelman (2002), Medusae Fossae Formation: New perspectives from Mars Global Surveyor, *J. Geophys. Res.*, *107*(E8), 5058, doi:10.1029/2001JE001537.

Breed, C. S., J. F. McCauley, and M. I. Whitney (1989), Wind erosion forms, in *Arid Zone Geomorphology*, edited by D. S. G. Thomas, pp. 284–307, Belhaven, London.

Burr, D. M., R. M. E. Williams, J. Nussbaumer, and J. R. Zimbelman (2006), Multiple, distinct (glacio?) fluvial paleochannels throughout the western Medusae Fossae Formation, Mars (abstract), *Proc. Lunar Planet. Sci. Conf.*, *36*, 1367.

Cas, R. A. F., and J. V. Wright (1992), *Volcanic Successions, Modern and Ancient: A Geological Approach to Processes, Products and Successions*, Chapman Hall, London.

Christensen, P., N. Gorelick, S. Anwar, S. Dickenshied, C. Edwards, and E. Engle (2007), New insights about Mars from the creation and analysis of Mars global data sets, *Eos Trans. AGU*, *88*(52), Fall Meet. Suppl., Abstract P11E–01.

Criswell, C. W., and W. E. Elston (1981), Morphological characteristics of terrestrial ash-flow tuff (ignimbrite) and related pyroclastic deposits, *Tech. Mem. TM-84211*, NASA, Washington, D. C.

Crown, D. A., and R. Greeley (1993), Volcanic geology of Hadriaca Patera and the eastern Hellas region of Mars, *J. Geophys. Res.*, *98*, 3431–3451.

Crown, D. A., R. Greeley, M. F. Sheridan, and R. Carrasco (1989), Analysis of an ignimbrite plateau in the Central Andes using LANDSAT thematic mapper data: Implications for the identification of ash deposits on Mars (abstract), *Proc. Lunar Planet. Sci. Conf.*, *20*, 206–207.

de Silva, S. L. (1989), Geochronology and stratigraphy of the ignimbrites from the 21°30′S to 23°30′S portion of the central Andes of northern Chile, *J. Volcanol. Geotherm. Res.*, *37*(2), 93–191, doi:10.1016/0377-0273(89)90065-6.

de Silva, S. L., G. Zandt, R. Trumbull, J. Viramonte, G. Salas, and N. Jimenez (2006), Large-scale silicic volcanism in the Central Andes—A tectonomagmatic phenomenon, *Geol. Soc. Spec. Publ.*, *269*, 47–64.

Edgett, K. S., B. J. Butler, J. R. Zimbelman, and V. E. Hamilton (1997), Geologic context of the Mars radar "Stealth" region in southwestern Tharsis, *J. Geophys. Res.*, *102*, 21,545–21,567, doi:10.1029/97JE01685.

Forsythe, R. D., and J. R. Zimbelman (1988), Is the Gordii Dorsum escarpment on Mars an exhumed transcurrent fault?, *Nature*, *336*(6195), 143–146, doi:10.1038/336143a0.

Francis, P. W., and C. A. Wood (1982), Absence of silicic volcanism on Mars: Implications for crustal composition and volatile abundance, *J. Geophys. Res.*, *87*(B12), 9881–9889, doi:10.1029/JB087iB12p09881.

Freundt, A., and H.-U. Schmincke (1995), Eruption and emplacement of basaltic welded ignimbrite during caldera formation on Gran Canaria, *Bull. Volcanol.*, *56*, 640–659.

Frey, H. V., S. E. H. Sakimoto, and J. H. Roarke (1998), MOLA topography and stratigraphy of geologic units at the dichotomy boundary: The Medusae Fossae Formation (abstract), *Proc. Lunar Planet. Sci. Conf.*, *29*, 1619.

Giordano, G., A. A. De Benedetti, A. Diana, G. Diano, F. Gaudioso, F. Marasco, M. Miceli, S. Mollo, R. A. F. Cas, and R. Funicello (2006), The Colli Albani mafic cladera (Roma, Italy): Stratigraphy, structure, and petrology, *J. Volcanol. Geotherm. Res.*, *155*, 49–80, doi:10.1016/j.jvolgeores.2006.02.009.

Glaze, L. S., and S. M. Baloga (2002), Volcanic plume heights on Mars: Limits of validity for convective models, *J. Geophys. Res.*, *107*(E10), 5086, doi:10.1029/2001JE001830.

Goudie, A. S. (2007), Mega-yardangs: A global analysis, *Geogr. Compass*, *1*, 65–81.

Greeley, R., and D. A. Crown (1990), Volcanic geology of Tyrrhena Patera, Mars, *J. Geophys. Res.*, *95*, 7133–7149.

Greeley, R., and J. E. Guest (1987), Geologic map of the eastern equatorial region of Mars, *U.S. Geol. Surv. Misc. Invest. Map*, *I-1802-B*.

Günster, N., P. Eck, A. Skowronek, and L. Zoller (2001), Late Pleistocene loess and their paleosols in the Granada Basin, Southern Spain, *Quat. Int.*, *76–77*, 241–245, doi:10.1016/S1040-6182(00)00106-3.

Head, J. W., and M. A. Kreslavsky (2001), Medusae Fossae Formation as volatile-rich sediments deposited during high obliquity: An hypothesis and tests, paper presented at Conference on the Geophysical Detection of Subsurface Water on Mars, Lunar and Planet. Inst., Houston, Tex., 6–10 Aug.

Head, J. W., and M. A. Kreslavsky (2004), Medusae Fossae Formation: Ice-rich airborne dust deposited during periods of high obliquity? (abstract), *Proc. Lunar Planet. Sci. Conf.*, *35*, 1635.

Hynek, B. M., R. E. Arvidson, and R. J. Phillips (2002), Explosive volcanism from Tharsis: Global evidence in the Martian geologic record (abstract), *Proc. Lunar Planet. Sci. Conf.*, *33*, 1408.

Hynek, B. M., R. J. Phillips, and R. E. Arvidson (2003), Explosive volcanism in the Tharsis region: Global evidence in the Martian geologic record, *J. Geophys. Res.*, *108*(E9), 5111, doi:10.1029/2003JE002062.

Inbar, M., and C. Risso (2001), Holocene yardangs in volcanic terrains in the southern Andes, Argentina, *Earth Surf. Processes Landforms*, *26*, 657–666, doi:10.1002/esp.207.

Ivanov, M. A., A. S. Kozyrev, M. L. Litvak, and I. G. Mitrofanov (2005), The Medusae Fossae-Elysium Region Mars: Geologic characteristics of the depression of epithermal-neutron flux based on HEND measurements onboard the *Mars Odyssey* spacecraft, *Sol. Syst. Res.*, *39*(1), 1–21.

Kadish, S. J., and N. G. Barlow (2006), Pedestal crater distribution and implications for a new model of formation, (abstract), *Proc. Lunar Planet. Sci. Conf.*, *37*, 1254.

Keller, J. M., W. V. Boynton, R. M. S. Williams, S. Karunatillake, and GRS Science Team (2006), Analysis of layering at Mars near-surface using attenuation of Chlorine gamma rays, (abstract), *Lunar Planet. Sci. Conf.*, *37*, 1184.

Lanagan, P. B., and A. S. McEwen (2003), Cerberus Plains volcanism: Constraints on temporal emplacement of the youngest flood lavas on Mars, paper presented at 6th International Conference on Mars, Lunar and Planet. Inst., Houston, Tex.

Malin, M. C. (1999), Oceans or seas in the Martian northern lowlands; high-resolution imaging tests of proposed coastlines, *Geophys. Res. Lett.*, *26*(19), 3049–3052, doi:10.1029/1999GL002342.

Malin, M. C., and K. S. Edgett (2000), Sedimentary rocks of early Mars, *Science*, *290*(5498), 1927–1937, doi:10.1126/science.290.5498.1927.

Malin, M. C., et al. (1998), Early views of the Martian surface from the Mars Orbiter Camera of Mars Global Surveyor, *Science*, *279*(5357), 1681–1685, doi:10.1126/science.279.5357.1681.

McCauley, J. F. (1973), Mariner 9 evidence for wind erosion in the equatorial and mid-latitude regions of Mars, *J. Geophys. Res.*, *78*, 4123–4137, doi:10.1029/JB078i020p04123.

McCauley, J. F., M. J. Grolier, and C. S. Breed (1977a), *Yardangs of Peru and Other Desert Regions (Interagency Report: Astrogeology)*, 177 pp., U.S. Geol. Surv., Reston, Va.

McCauley, J. F., C. S. Breed, and M. J. Grolier (1977b), Yardangs, in *Geomorphology in Arid Regions*, edited by D. O. Doehring, pp. 233–269, Allen and Unwin, Boston.

McColley, S. M., J. W. Head, and G. Neukum (2005), The Medusae Fossae Formation: Geological characteristics and topographic and stratigraphic relationships of the lower member along southeastern Elysium Planitia (abstract), *Proc. Lunar Planet. Sci. Conf.*, *36*, 1184.

Mouginis-Mark, P. (1993), The influence of oceans on Martian volcanism (abstract), *Proc. Lunar Planet. Sci. Conf.*, *24*, 1021–1022.

Nussbaumer, J. (2005), Extent and further characteristics of former glaciated terrain in Elysium Planitia, Mars (abstract), *Proc. Lunar Planet. Sci. Conf.*, *36*, 1949.

Nussbaumer, J., R. Jaumann, and E. Hauber (2003), Evidence for a surging ice sheet in Elysium Planitia, Mars, paper presented at 6th International Conference on Mars, Lunar and Planet. Inst., Houston, Tex.

Parker, T. J. (1991), A comparison of the Martian Medusae Fossae Formation with terrestrial carbonate platforms (abstract), *Proc. Lunar Planet. Sci. Conf.*, *22*, 1029 – 1030.

People's Republic of China (1982), *30 Years' Review of China's Science and Technology, 1949 – 79*, World Sci., Hackensack, N. J.

Roever, W. P. D. E. (1966), Dacitic ignimbrites with upward increasing compactness near Sibolangit (NE Sumatra, Indonesia) and their peculiar hydrology, *Bull. Volcanol.*, *29*, 105 – 122, doi:10.1007/BF02597147.

Ross, C. S., and R. L. Smith (1961), Ash-flow tuffs: Their origin, geologic relations, and identification, *U.S. Geol. Surv. Prof. Pap.*, *366*, 1 – 81.

Sakimoto, S. E. H., H. V. Frey, J. B. Garvin, and J. H. Roark (1999), Topography, roughness, layering, and slope properties of the Medusae Fossae Formation from Mars Orbiter Laser Altimeter (MOLA) and Mars Orbiter Camera (MOC) data, *J. Geophys. Res.*, *104*(E10), 24,141 – 24,154.

Schultz, P. H., and A. B. Lutz (1988), Polar wandering on Mars, *Icarus*, *73*, 91 – 141, doi:10.1016/0019-1035(88)90087-5.

Scott, D. H., and K. L. Tanaka (1982), Ignimbrites of Amazonis Planitia region of Mars, *J. Geophys. Res.*, *87*, 1179 – 1190, doi:10.1029/JB087iB02p01179.

Scott, D. H., and K. L. Tanaka (1986), Geologic map of the western equatorial region of Mars, *U.S. Geol. Surv. Misc. Invest. Map*, *I-1802-A*.

Selby, M. J., P. Augustinus, V. G. Moon, and R. J. Stevenson (1988), Slopes on strong rock masses: Modeling and influences of stress distribution and geomechanical properties, in *Modelling Geomorphological Systems*, edited by M. G. Anderson, pp. 341 – 374, John Wiley, Hoboken, N. J.

Smith, D. E., et al. (1999), The global topography of Mars and implications for surface evolution, *Science*, *284*, 1495 – 1503, doi:10.1126/science.284.5419.1495.

Takagi, M., and J. R. Zimbelman (2001), Geomorphic mapping and analysis of the eastern Medusae Fossae Formation, Mars (abstract), *Proc. Lunar Planet. Sci. Conf.*, *32*, 1579.

Tanaka, K. L. (2000), Dust and ice deposition in the Martian geologic record, *Icarus*, *144*, 254 – 266, doi:10.1006/icar.1999.6297.

Tanaka, K. L., and G. J. Leonard (1998), Martian paleopolar deposits: Evidence for a stable pole and periods of climate change, paper presented at 1st International Conference on Mars Polar Science and Exploration, Lunar and Planet. Inst., Camp Allen, Tex.

Tramp, K. L., G. S. Soreghan, and R. D. Elmore (2004), Paleoclimatic inferences from paleopedology and magnetism of the Permian Maroon Formation loessite, Colorado, USA, *Geol. Soc. Am. Bull.*, *116*, 671 – 686, doi:10.1130/B25354.1.

Ward, A. W. (1979), Yardangs on Mars: Evidence of recent wind erosion, *J. Geophys. Res.*, *84*, 8147 – 8166, doi:10.1029/JB084iB14p08147.

Ward, A. W., and R. Greeley (1984), Evolution of yardangs at Roger Lake, California, *Geol. Soc. Am. Bull.*, *95*, 829 – 837, doi:10.1130/0016-7606(1984)95<829:EOTYAR>2.0.CO;2.

Watters, T. R., et al. (2007), Radar sounding of the Medusae Fossae Formation, Mars: Equatorial ice, or dry, low-density deposits, *Science*, *318*, 1125 – 1128.

Wilson, L., and J. W. Head (1994), Mars: Review and analysis of volcanic eruption theory and relationships to observed landforms, *Rev. Geophys.*, *32*, 221 – 264.

Wyrick, D., D. A. Ferrill, A. P. Morris, S. L. Colton, and D. W. Sims (2004), Distribution, morphology, and origins of Marian pit crater chains, *J. Geophys. Res.*, *109*, E06005, doi:10.1029/2004JE002240.

Zimbelman, J. R. (2003), Evidence supporting an ignimbrite origin for the Medusae Fossae Formation, Mars, *Geol. Soc. Am. Abstr. Programs*, *35*, 265.

Zimbelman, J. R., and S. D. Patel (1998), Photogeologic constraints on the emplacement of the Medusae Fossae Formation, Mars (abstract), *Lunar Planet. Sci. Conf.*, *29*, 1085.

Zimbelman, J. R., D. Crown, and D. Jenson (1996), Initial investigation of the enigmatic massive deposits in Amazonis Planitia, Mars (abstract), *Proc. Lunar Planet. Sci. Conf.*, *27*, 1495.

Zimbelman, J. R., D. A. Crown, J. A. Grant, and D. M. Hooper (1997a), The Medusae Fossae Formation, Amazonis Planitia, Mars: Evaluation of proposed hypotheses of origin (abstract), *Proc. Lunar Planet. Sci. Conf.*, *28*, 1482.

Zimbelman, J. R., A. K. Johnston, P. S. Russell, and C. G. Lovett (1997b), Regional geologic setting of the Medusae Fossae Formation on Mars, *Eos Trans. AGU*, *78*(46), 411.

Zimbelman, J. R., S. E. H. Sakimoto, and H. Frey (2000), Evidence for a fluvial contribution to the complex story of the Medusae Fossae Formation on Mars, *Geol. Soc. Am. Abstr. Programs*, *32*, 303.

Zimbelman, J. R., K. C. Bender, and J. C. Harris (2003), Geologic mapping applications using THEMIS data for the Medusae Fossae Formation, Mars (abstract), *Proc. Lunar Planet. Sci. Conf.*, *34*, 1390.

D. A. Crown, Planetary Science Institute, 1700 East Fort Lowell Road, Suite 106, Tucson, AZ 85719, USA.

S. L. de Silva, Department of Geosciences, Oregon State University, 104 Wilkinson Hall, Corvallis, OR 97331, USA.

K. E. Mandt, Space Science and Engineering Division, Southwest Research Institute, 6220 Culebra Road, P.O. Drawer 28510, San Antonio, TX 78228, USA. (kathymandt@yahoo.com)

J. R. Zimbelman, Center for Earth and Planetary Sciences, National Air and Space Museum, Smithsonian Institution, P.O. Box 37012, MRC 315, Washington, DC 20013, USA.